AFRL-ML-WP-TP-2006-419

EFFECT OF INCLUSION MORPHOLOGY ON THE COEFFICIENT OF THERMAL EXPANSION IN FILLED EPOXY MATRIX (PREPRINT)

Kaushik Mallick, John Cronin, and Steven Arzberger

APRIL 2006

Approved for public release; distribution is unlimited.

STINFO COPY

MATERIALS AND MANUFACTURING DIRECTORATE
AIR FORCE RESEARCH LABORATORY
AIR FORCE MATERIEL COMMAND
WRIGHT-PATTERSON AIR FORCE BASE, OH 45433-7750

NOTICE AND SIGNATURE PAGE

Using Government drawings, specifications, or other data included in this document for any purpose other than Government procurement does not in any way obligate the U.S. Government. The fact that the Government formulated or supplied the drawings, specifications, or other data does not license the holder or any other person or corporation; or convey any rights or permission to manufacture, use, or sell any patented invention that may relate to them.

This report was cleared for public release by the Air Force Research Laboratory Wright Site (AFRL/WS) Public Affairs Office and is available to the general public, including foreign nationals. Copies may be obtained from the Defense Technical Information Center (DTIC) (http://www.dtic.mil).

AFRL-ML-WP-TP-2006-419 HAS BEEN REVIEWED AND IS APPROVED FOR PUBLICATION IN ACCORDANCE WITH ASSIGNED DISTRIBUTION STATEMENT.

*//Signature//

VERNON BECHEL, Program Manager
Structural Materials Branch
Nonmetallic Materials Division

//Signature//

TIA BENSON TOLLE, Chief
Structural Materials Branch
Nonmetallic Materials Division

//Signature//

SHASHI K. SHARMA, Acting Deputy Chief
Nonmetallic Materials Division
Materials and Manufacturing Directorate

This report is published in the interest of scientific and technical information exchange, and its publication does not constitute the Government's approval or disapproval of its ideas or findings.

*Disseminated copies will show "//Signature//" stamped or typed above the signature blocks.

REPORT DOCUMENTATION PAGE

Form Approved
OMB No. 0704-0188

1. REPORT DATE *(DD-MM-YY)*	2. REPORT TYPE	3. DATES COVERED *(From - To)*
April 2006	Conference Paper Preprint	

4. TITLE AND SUBTITLE
EFFECT OF INCLUSION MORPHOLOGY ON THE COEFFICIENT OF THERMAL EXPANSION IN FILLED EPOXY MATRIX (PREPRINT)

5a. CONTRACT NUMBER
HQ0006-04-C-7070

5b. GRANT NUMBER

5c. PROGRAM ELEMENT NUMBER
N/A

6. AUTHOR(S)
Kaushik Mallick, John Cronin, and Steven Arzberger

5d. PROJECT NUMBER
N/A

5e. TASK NUMBER
N/A

5f. WORK UNIT NUMBER
N/A

7. PERFORMING ORGANIZATION NAME(S) AND ADDRESS(ES)
Composite Technology Development, Inc.
Lafayette, CO, 80026

8. PERFORMING ORGANIZATION REPORT NUMBER

9. SPONSORING/MONITORING AGENCY NAME(S) AND ADDRESS(ES)
Materials and Manufacturing Directorate
Air Force Research Laboratory
Air Force Materiel Command
Wright-Patterson AFB, OH 45433-7750

10. SPONSORING/MONITORING AGENCY ACRONYM(S)
AFRL-ML-WP

11. SPONSORING/MONITORING AGENCY REPORT NUMBER(S)
AFRL-ML-WP-TP-2006-419

12. DISTRIBUTION/AVAILABILITY STATEMENT
Approved for public release; distribution is unlimited.

13. SUPPLEMENTARY NOTES
This work has been submitted to AIAA for publication in the Proceedings of the 48th Structures, Structural Dynamics, and Materials (SDM) Conference. One or more of the authors is a U.S. Government employee working within the scope of their Government job; therefore, the U.S. Government is joint owner of the work. If published, AIAA may assert copyright. The Government has the right to copy, distribute, and use the work. All other rights are reserved by the copyright owner.

This paper contains color. PAO Case Number: AFRL/WS 06-0825, 30 Mar 2006.

14. ABSTRACT
The paper presents material development research performed at Composite Technology Development, Inc. towards optimization of the design for linerless composite cryogenic tanks. In a cryogenic composite tank, large thermal strains develop through the thickness of the tank laminate due to the mismatch in the coefficient of thermal expansion of adjacent plies with different fiber orientations. These thermal strains are primarily caused by the thermal contraction of the matrix material. Excessive thermal strains can cause microcracks in the matrix and inter-ply delamination, leading to leakage of the fluid contained by the tank. Reduction of the thermal expansion of the matrix is viewed as an essential design tool for optimizing these tanks. Addition of inclusions that are much stiffer than the matrix is an effective means to reduce thermal expansion of the matrix for the composite, as long as it doesn't compromise the toughness. The paper presents an analytical scheme to predict the effective thermal expansion properties of the filled matrix with embedded inclusions and investigates the effect of inclusion morphology, shape and aspect ratio on the same. The analytical predictions are compared with actual test results of thermal expansion measured for the matrix. The inductions and trends are being used to select the best material and to improve their processing to achieve the most optimized cryogenic tank design.

15. SUBJECT TERMS
cryogenic composite tank, thermal strains, matrix, thermal expansion properties

16. SECURITY CLASSIFICATION OF:			17. LIMITATION OF ABSTRACT:	18. NUMBER OF PAGES	19a. NAME OF RESPONSIBLE PERSON (Monitor)
a. REPORT	b. ABSTRACT	c. THIS PAGE			Vernon Bechel
Unclassified	Unclassified	Unclassified	SAR	16	19b. TELEPHONE NUMBER *(Include Area Code)* N/A

Effect of Inclusion Morphology on the Coefficient of Thermal Expansion in Filled Epoxy Matrix

Kaushik Mallick[*], John Cronin[†] and Steven Arzberger[‡]
Composite Technology Development, Inc., Lafayette, Colorado, 80026

Abstract

The paper presents material development research performed at Composite Technology Development, Inc. towards optimization of the design for linerless composite cryogenic tanks. Specifically, it presents both analytical and experimental work towards reducing the thermal expansion of epoxy matrix for composite materials. In a cryogenic composite tank, large thermal strains develop through the thickness of the tank laminate due to the mismatch in the coefficient of thermal expansion of adjacent plies with different fiber orientations. These thermal strains are primarily caused by the thermal contraction of the matrix material. Excessive thermal strains can cause microcracks in the matrix and inter-ply delamination, leading to leakage of the fluid contained by the tank. Therefore, reduction of the thermal expansion of the matrix is viewed as an essential design tool for optimizing these tanks. Addition of inclusions that are much stiffer than the matrix is an effective means to reduce thermal expansion of the matrix for the composite, as long as it doesn't compromise the toughness. The paper presents an analytical scheme to predict the effective thermal expansion properties of the filled matrix with embedded inclusions and investigates the effect of inclusion morphology, shape and aspect ratio on the same. The analytical predictions are compared with actual test results of thermal expansion measured for the matrix. The inductions and trends from analytical computations are being used to select the best material and to improve their processing to achieve the most optimized cryogenic tank design.

Nomenclature

α	=	aspect ratio of the inslusion
α_m	=	coefficient of thermal expansion of the matrix
α_c	=	coefficient of thermal expansion of the filled matrix
C_m	=	elastic stiffness tensor of the matrix
C_f	=	elastic stiffness tensor of the inclusion
$\bar{e}$	=	average strain in the matrix
f	=	volume fraction of the inclusion
I	=	identity tensor
S	=	Eshelby Tensor
T	=	transformation tensor
ΔP	=	pressure differential through the tank laminate
ξ	=	empirical constant in permeability testing

[*] Senior Project Manager, Kaushik@CTD-materials.com, email: *kaushik@ctd-materials.com*, AIAA member
[†] Design Engineer
[‡] Senior Chemist

I. Motivation

Linerless composite cryogenic tanks are being considered by the Department of Defense for applications that can benefit from the weight, cost, and schedule advantages that these structures offer.[1] Because of their lower launch mass, fewer part count, and quick manufacturing turn-around time, linerless composite tanks will be enabling for launch vehicles, especially in their upper stages, for the 'Operationally Responsive Space Launch Initiative'. It has been estimated that the use of composite tanks will offer up to 40 percent weight reduction compared to current conventional metallic tanks, allowing increased payload capability and/or reduced launch mass. Ultra-lightweight linerless composite tanks have also been identified by NASA as enabling for future reusable launch vehicles and in-space propulsion systems (Figure 1).[2]

Although composite materials hold much promise for lightweight tanks, their adoption has been slowed by concerns over structural integrity and material compatibility.[3] Conventional composite materials typically become brittle and suffer from microcracking when exposed to cryogenic temperatures, leading to tank leakage or structural failure. The use of carbon fiber based composites in cryogenic applications has been explored for the last 20 years. [3] However, it is only very recently that more novel and advanced composite materials have been developed and characterized well enough to make them viable alternative to metallic materials in cryogenic fuel tanks. The properties of these new materials must be explored further so that they can be used with confidence and to encourage more advances to be made in future material development efforts.

Figure 1: Linerless composite tanks will enable several future missions such as launch vehicles for Responsive Space (left) and reusable Crew Exploration Vehicles (right)

One of the technical challenges in placing composites in a cryogenic environment is to choose and / or design the material to resist the proliferation of microcracks that may lead to leakage through the wall of the tank within the tank's operating regime. Several studies in the past have focused on how composites microcrack and leak when they are thermally cycled between cryogenic and elevated temperatures.[4-10] Most of the research conclude that microcracks are caused by large thermal stresses that develop through the thickness of the tank laminate due to the mismatch in the coefficient of thermal expansion (CTE) of adjacent plies with different fiber orientations. Since the CTE of the polymer matrix is much higher than that of the unidirectional fibers, the transverse microcracks are initiated in plies that want to shrink across the fiber direction but are restrained by their neighboring plies.

The design of a typical composite tank requires a laminate design that is inherently anisotropic, resulting in the CTE mismatch between the adjacent plies. The feasible design optimization space that aims to minimize the tank weight and at the same time mitigate microcracking by manipulating the laminate architecture is very limited.[11] This leaves the cryogenic tank designer with two possible design routes to mitigate microcracking in the tank wall, both being dependent on material development: 1. improve the microcrack fracture toughness and 2. reduce the thermal expansion coefficient of the matrix material to minimize the amount of residual stresses at cryogenic temperature. The two efforts usually have conflicting demands on material design and formulation. Tremendous progress has been made to date at CTD in developing novel composite materials with microcrack resistance significantly better than common off-the-shelf materials.[1] The current paper focuses on the second option i.e. reduction of the CTE of the matrix through judicious choice of inclusions. Specifically the paper aims to achieve three objectives: 1. identify the morphology of the inclusion that would give the best reduction in CTE, 2. correlate with experimental measurement of CTE of inclusion reinforced matrix and 3. optimize the reinforcement volume fraction to achieve the desired performance.

II. Effective CTE of Epoxy Matrix with Embedded Inclusions

A. Model for Calculating the Effective CTE

The analytical framework used in the current paper for the prediction of CTE is based on the mean field theory. The mean field theory is a continuum mechanics based approach aimed at homogenization of multiphase

materials.[13,14] It is used for example in deducing their overall ("effective" or "apparent") behavior (e.g. stiffness, thermal expansion and strength properties, heat conduction and related transport properties, electrical and magnetic properties, electromechanical properties, …) from the corresponding material behavior of the constituents (and of the interfaces between them) and from the geometrical arrangement of the phases.[13,13] The theory is based on the assumption of equivalence of the strain energy of the actual solid with a disordered microstructure and that of an appropriately defined effective continuum.[14]

The model for computing the effective CTE of a matrix embedded with inclusions is shown in Figure 2. The inclusions are assumed to be of the same size and ellipsoidal shape, with an aspect ratio of α=a/R and transversely isotropic properties. This approach allows the computation to be very flexible and generalized to take into account a wide variety of reinforcement morphology - (a) platelet or disc when α<1, (b) short fiber or whisker for α>1 and (c) spherical when α=1. Takao and Taya[15] and Takao[16] had used the Eshelby's equivalent inclusion method to predict CTE of the short fiber/whisker reinforced matrix material. This analytical approach is extended in the current effort to include platelet like reinforcement as well as spherical reinforcement. In addition the analytical derivations of the effective CTE presented in the proposed paper take into account the random distribution of the inclusions as well as the anisotropy of both mechanical and thermal properties of the inclusions unlike the previous effort.

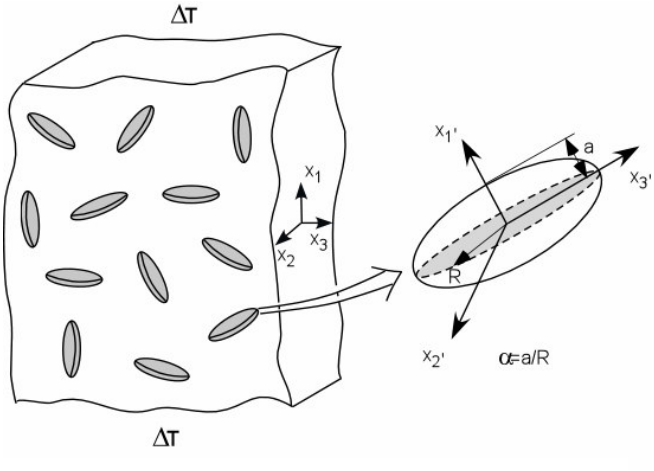

Figure 2: A model for calculating the effective CTE of an inclusion reinforced matrix

The effective CTE of the reinforced matrix is derived as:[15,16]

$$\alpha_c = \alpha_m - f\int \langle TG_3T^{-1}\rangle dV \bullet \bar{e} + f\int \langle TG_4\Delta\alpha\rangle dV \tag{1}$$

where,

$$\Delta\alpha = \alpha_f - \alpha_m \tag{2}$$

α_c and α_m being the CTE of the inclusion and the matrix respectively, and

$$\begin{aligned} G_3 &= \{[(C_f - C_m)(S - I) + C_f\}^{-1}(C_f - C_m) \\ G_4 &= \{[(C_f - C_m)(S - I) + C_f\}^{-1} C_f \end{aligned} \tag{3}$$

C_f, C_m are the elastic stiffness tensors for the inclusion and the matrix, *I* is an identity tensor and *S* is the Eshelby tensor . The different terms of the Eshelby tensor *S(i,j)* are provided in Appendix A.

In eqn. (1), $\bar{e}$ defines the average strain in the matrix due to thermal shrinkage and is obtained by solving the following simultaneous equations:

$$\left(I - f\int \langle TG_1T^{-1}\rangle dV\right)\bullet \bar{e} + f\int \langle TG_2\Delta\alpha\rangle dV = 0 \tag{4}$$

where,

$$\begin{aligned} G_1 &= (S - I)G_3 \\ G_2 &= (S - I)G_4 \end{aligned} \tag{5}$$

In both eqns (1) and (4), *T* represents the transformation matrix provided in Appendix B and the terms $\langle x\rangle$ represent orientation average of the tensor *x* to account for the random orientation distribution of the inclusions in the matrix.[17]

$$\langle x\rangle = \frac{1}{2\pi^2}\int_{-\pi}^{\pi}\int_{0}^{\pi}\int_{0}^{\pi/2} x\sin(\alpha_2)\,d\alpha_1 d\alpha_2 d\alpha_3 \tag{6}$$

B. Calculation of Effective CTE

Sample calculations are performed to determine the effective CTE of the embedded matrix for different types of inclusions. Representative material properties, shapes and aspect ratios assumed for the inclusions are listed in Table 1. In the results presented, the effective CTE of the embedded matrix is normalized with respect to the virgin matrix CTE. Also since the mean field theory based derivation of the effective CTE assumes only a semi-dilute concentration of the inclusions, the volume fraction of the fillers is been limited to 30%. This limit was chosen arbitrarily, but more specific limits will be derived in the near future based on percolation thresholds of inclusion connectivity.[18, 19]

Table 1: Elastic properties and thermal expansion coefficients used in the calculations

Material	Inclusion shape & aspect ratio	Elastic properties				Thermal properties	
		E_L	E_T	ν_{LT}	G_{LT}	α_L	α_T
		GPa	GPa		GPa	10^{-6} mm/mm/K	10^{-6} mm/mm/K
CTD 500XA epoxy matrix	-	3.4	3.4	.36	1.24	30.0	30.0
Nanofibers	Rod, α=300	400.0	40.0	.2	16.0	-1.0	27.0
Silica	Spherical, α=1	70.0	70.0	.2	29.16	5.0	5.0
Nanoclay	Disk, α=.001	176.0	176.0	.2	73.3	3.0	3.0
Zirconium Tungstate	Spherical, α=1	200.0	200.0	.3	76.92	-7.2	-7.2
Kevlar whiskers	Rod, α=300	61.0	4.2	.35	2.9	-2.0	30.0
PBO whiskers	Rod, α=300	270.0	30.0	.3	13.5	-6.0	50

C. Effect of Inclusion Properties on Effective CTE

Figure 3 compares the effective CTE of the matrix material reinforced with several different types of inclusions – silica (spherical particles), nanofiber (rod shaped), nanoclay (disk-shaped), Kevlar whiskers (rod shaped) and PBO whiskers (rod shaped). All three of the rod shaped inclusions were chosen because of their negative axial CTE and strongly anisotropic properties. The effective CTE of the filled matrix was found to be quite different for these three fibers, since the elastic as well as thermal properties for these fibers play a role in the effective CTE calculation. For spherical and isotropic silica inclusions, the results indicate a linear dependency of the effective CTE on the volume fraction since it coincides with the prediction of a simple rule of mixture. Of all the different inclusions the nanofiber shows the best promise in CTE reduction.

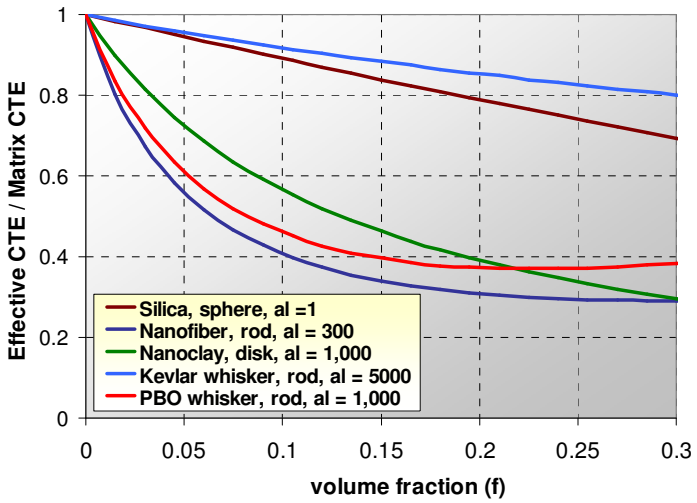

Figure 3: Effective CTE of epoxy matrix reinforced by different kinds of inclusions.

D. Effect of Inclusion Orientation on Effective CTE

Figure 4 shows the variation of effective CTE of the matrix material reinforced by nanofibers which are strongly anisotropic in their elastic as well as thermal properties (see Table 1). The calculations are performed for two different inclusion arrangements – parallel array and random. For the former case, the effective CTE of the material in the longitudinal direction (same as the fiber axial arrangement) is significantly lower but the CTE in the transverse direction is found to be higher than that of the base matrix material for small volume fraction of the inclusions. Such behavior is caused by the axial constraint enforced by the stiff fibers. On heating the composite (matrix + inclusion), axial expansion of the matrix is strongly inhibited and the resultant axial compression of the matrix generates a Poisson's expansion in the transverse direction, which more than compensates for the reduction in natural transverse thermal expansion induced by the presence of the fibers.[20] Similar results have been predicted in the past literature.[15,16] The MFT estimates a 90% reduction in effective CTE along the preferred orientation for a parallel array and a 45% reduction for random dispersion of the nanofibers, both for a 5% volume fraction of inclusions, which far exceeds the expectations of a rule of mixtures. These results also indicate that the type of orientation of the inclusions which can be influenced by the processing conditions, is an important factor to consider for estimating the effective thermal properties.

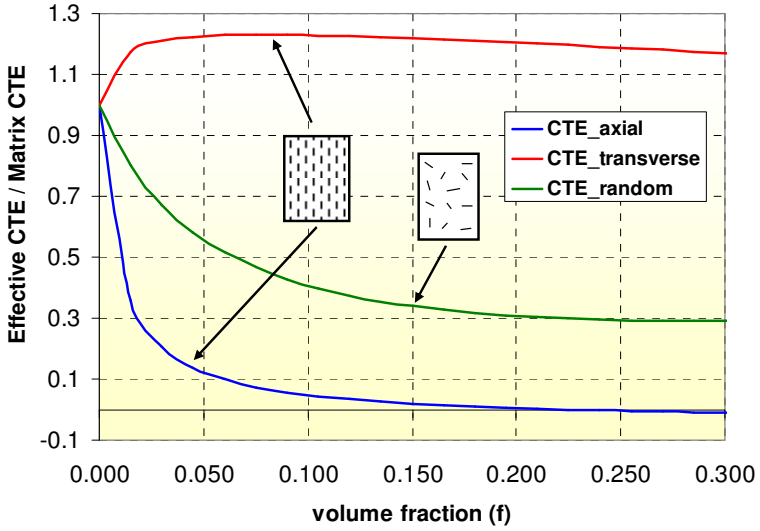

Figure 4: Effect of orientation on the CTE of nanofiber reinforced epoxy matrix

E. Effect of Inclusion Aspect Ratio on Effective CTE

The expected reduction in the effective CTE of the matrix reinforced by nanofiber is due to the strong anisotropy of the fibers, its negative CTE along the axial direction of the fibers as well as its high aspect ratio (300~1000). There has been concern that good dispersion of these fibers in the matrix will necessitate high shear mixing which can possibly reduce the aspect ratio by breaking the individual fibers during mixing. Figure 5 shows the effective CTE of the reinforced matrix for different aspect ratios of nanofibers. The influence on the effective CTE is much more significant when the aspect ratio is reduced from α=100 to α=10 than it is from α=1000 to α=100. The trend suggests that it is extremely important to control or preserve the aspect ratio of the fibers during processing or mixing if the promised CTE reduction is to be realized.

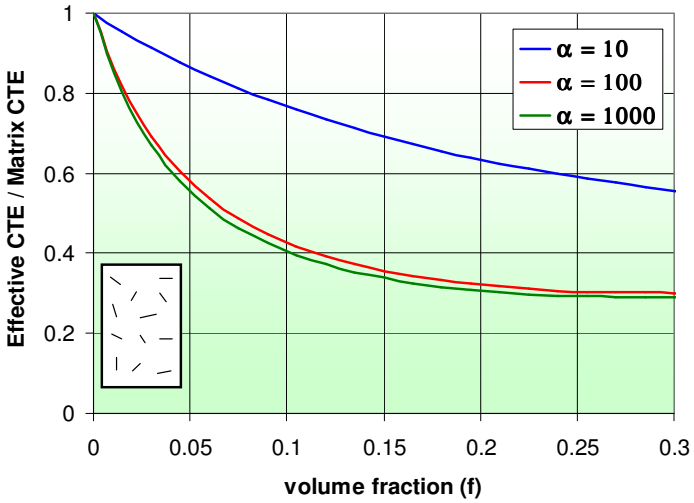

Figure 5: Effect of aspect ratio on the effective CTE of nanofiber reinforced epoxy matrix

F. Effect of Inclusion Shape on Effective CTE

There has been tremendous interest in Zirconium Tungstate (ZrW_2O_8), a ceramic with a strongly negative coefficient of thermal expansion (CTE). In contrast to most other ceramics exhibiting negative CTE, the CTE of ZrW_2O_8 is isotropic and has a large negative magnitude (average CTE of -7.2 x 10^{-6} mm/mm/K) over a wide range of temperature (0K to 1050 K).[21-23] These unusual properties suggest the incorporation of ZrW_2O_8 into a polymeric matrix, to create a composite with very low CTE. The objective of the computation performed here is to illustrate that the inclusion shape is an important consideration, more so than its negative CTE in order to achieve a matrix material with low CTE. Figure 6 shows that incorporating spherical ZrW_2O_8 particles reduces the effective CTE only moderately, following a rule of mixture as expected. However, significant CTE reduction can be achieved if the ZrW_2O_8 ceramic can be processed in the shape of either whiskers or platelets. The more pronounced the aspect ratio, the stronger the CTE reduction. The computations also show that for random dispersion of a given type of inclusion, the most reduction in the effective CTE is obtained with the disk shaped inclusions.

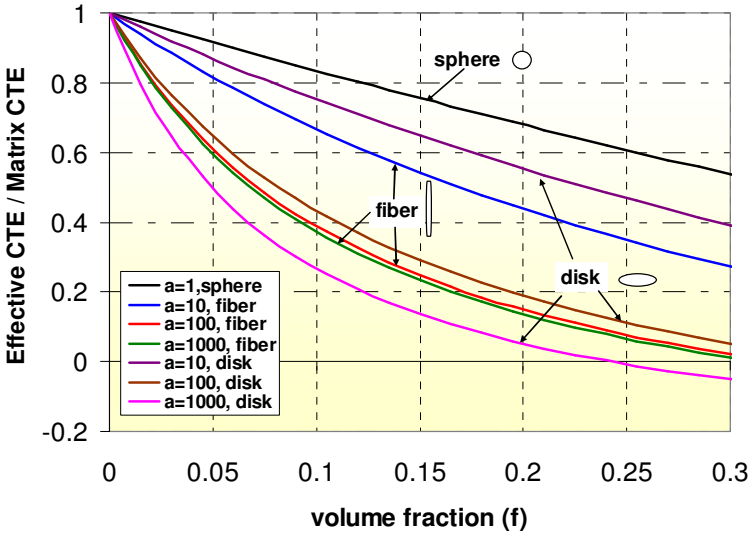

Figure 6: Effect of inclusion shape on the effective CTE

III. Experimental Results

A. Measurement of Thermal Strain

Specimens for measuring thermal strain were prepared from flat plates of CTD-500XA epoxy resin reinforced with different weight fractions of nanofibers. 32mm x 32mm square test specimens were cut, prepared and strain-gaged. Thermal expansion tests were performed using a CTD designed test set-up that uses cryogenic strain gages and a comparative strain analysis technique developed by National Institute of Standards and Technology (NIST). The NIST traceable standards used in the test for comparison were copper and borosilicate glass specimens. The thermal expansion was recorded from liquid Nitrogen temperature (77 K) to room temperature (293 K). Each sample was tested 5 times and the results were averaged.

Figure 7 compares the experimentally measured thermal strain of the matrix embedded with different weight fractions of nanofibers and the virgin matrix material. The results of the tests show that nanofibers have the potential to significantly reduce the thermal expansion of the base matrix material. There is an overall reduction of 24.6% in the thermal expansion of the matrix using 12% by weight of nanofiber. A summary of the test results that compare the reduction achieved in total thermal expansion at 77K for different concentrations of nanofibers can be seen in Figure 8.

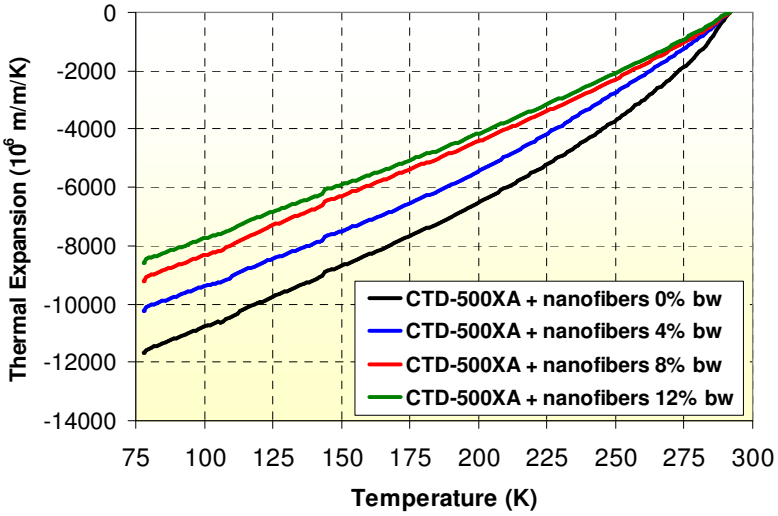

Figure 7: Thermal expansion of nanofiber reinforced CTD-500XA measured from 77 K to 293 K.

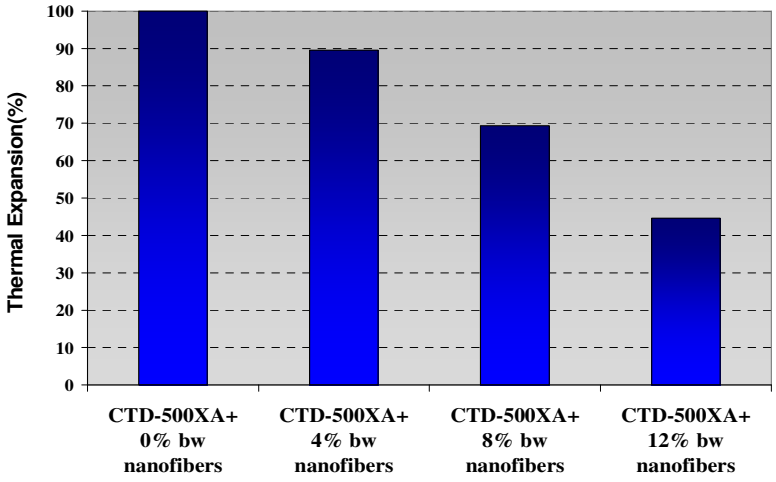

Figure 8: Reduction of thermal expansion with different weight fractions of nanofiber inclusion

B. Comparison with Analytical Prediction

Figure 9 compares the experimentally measured CTE of the nanofiber reinforced matrix with the analytical predictions. The effective CTE of the matrix at room temperature (293K) was computed from the slope of the thermal expansion plot (Figure 7). Two different aspect ratios of the rod-shaped nanofibers were considered: α=10 and α=100. Assuming that, the experimental results agree fairly with the analytical predictions for α=10 for volume fraction less than 2.5%. It may be conjectured that the aspect ratio of the nanofibers is significantly reduced during the processing from its initial aspect ration of aspect ratio of $\alpha \approx 300$. The nonlinear trend in the CTE reduction is encouraging, with a steeper drop for increasing concentration of nanofibers. The analytical solution is limited to dilute concentration of inclusions and is valid until the interaction effect between the nanofibers start to dominate. The ensuing phenomenon needs to be studied under the light of percolation theory.[17]

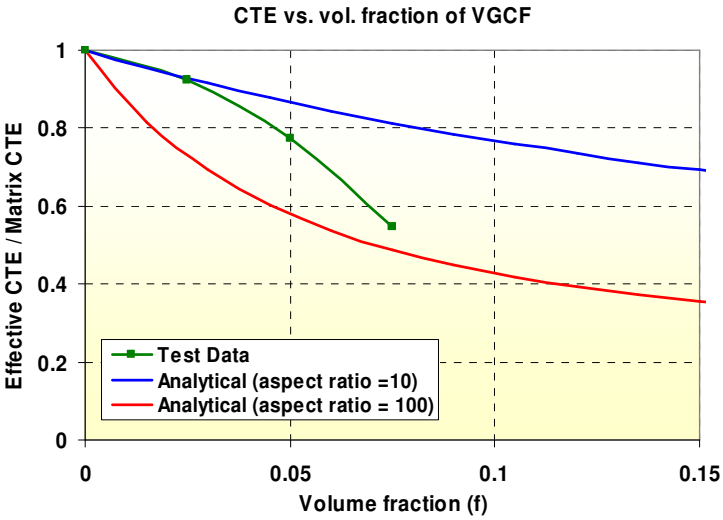

Figure 9: CTE of nanofiber reinforced matrix at room temperature (293K)

IV. Summary

Microcracking in composite laminates subjected to thermal loads is an obstacle to the development of linerless composite cryogenic tanks. Microcracks are a result of large thermal strains that develop through the thickness of the tank laminate due to the mismatch in the coefficient of thermal expansion of adjacent plies with different fiber orientations. The paper presented both analytical and experimental work towards reducing the CTE of epoxy matrix for composite materials by adding inclusions that are much stiffer than the matrix. An analytical model is first used to predict the reduction in the CTE of the matrix embedded with dilute concentrations of inclusions. The effect of the shape, aspect ratio and arrangement of the inclusions on the effective CTE of the matrix is investigated systematically. The trends in the CTE reduction derived from analytical calculations are used to select the best type of inclusions for material development efforts. Experiments are performed to measure the thermal expansion in matrix embedded with nanofibers from room temperature to cryogenic temperature. Test results demonstrate significant reduction of the thermal expansion for moderate volume fractions of nanofibers. Finally, the effective CTE of the matrix is compared with analytical predictions and inferences are made on their agreement.

Appendix A. Eshelby Tensors

The Eshelby tensor *S(i,j)* is defined by:

$$S(1,1)=\frac{1}{2(1-\nu_m)}\left\{\frac{4\alpha^2-2}{\alpha^2-1}-2\nu_m+\left[\frac{4\alpha^2-1}{1-\alpha^2}+2\nu_m\right]g(\alpha)\right\}$$

$$S(2,2)=S(3,3)=\frac{1}{4(1-\nu_m)}\left\{\frac{3\alpha^2}{2(\alpha^2-1)}+\left[\frac{4\alpha^2-13}{4(\alpha^2-1)}-2\nu_m\right]g(\alpha)\right\}$$

$$S(1,2)=S(1,3)=\frac{1}{2(1-\nu_m)}\left\{\frac{\alpha^2}{1-\alpha^2}+2\nu_m+\left[\frac{2\alpha^2+1}{2(\alpha^2-1)}-2\nu_m\right]g(\alpha)\right\}$$

$$S(2,1)=S(3,1)=\frac{1}{4(1-\nu_m)}\left\{\frac{2\alpha^2}{1-\alpha^2}+\left[\frac{2\alpha^2+1}{\alpha^2-1}+2\nu_m\right]g(\alpha)\right\}$$

$$S(2,3)=S(3,2)=\frac{1}{4(1-\nu_m)}\left\{\frac{\alpha^2}{2(\alpha^2-1)}+\left[\frac{4\alpha^2-1}{4(1-\alpha^2)}+2\nu_m\right]g(\alpha)\right\}$$

$$S(4,4)=S(5,5)=\frac{1}{2(1-\nu_m)}\left\{\frac{2}{1-\alpha^2}-2\nu_m+\frac{1}{2}\left[\frac{2\alpha^2+4}{\alpha^2-1}+2\nu_m\right]g(\alpha)\right\}$$

$$S(6,6)=\frac{1}{2(1-\nu_m)}\left\{\frac{\alpha^2}{2(\alpha^2-1)}+\left[\frac{4\alpha^2-7}{4(\alpha^2-1)}-2\nu_m\right]g(\alpha)\right\} \qquad \text{(A7)}$$

all other components of $S(i,j)$ being zero. The function $g(\alpha)$ is defined as

$$g(\alpha)=\frac{\alpha}{(\alpha^2-1)^{3/2}}\left[\alpha(\alpha^2-1)^{1/2}-\cosh^{-1}(\alpha)\right] \quad \text{for } \alpha>1 \text{ (whiskers/fibers)} \qquad \text{(A2)}$$

$$g(\alpha)=\frac{\alpha}{(1-\alpha^2)^{3/2}}\left[\cos^{-1}(\alpha)-\alpha(1-\alpha^2)^{1/2}\right] \text{ for } \alpha<1 \text{ (platelets/disks)} \qquad \text{(A3)}$$

For $\alpha=1$ (spherical inclusions), the components of $S(i,j)$ can be calculated by limit investigation for $i,j\le 3$ as

$$S(i,i)=\frac{7-5\nu_m}{15(1-\nu_m)}$$
$$S(i,j)=-\frac{1-5\nu_m}{15(1-\nu_m)} \qquad \text{for } i\neq j \qquad \text{(A4a)}$$

and

$$S(i,i)=\frac{8-10\nu_m}{15(1-\nu_m)} \qquad \text{for } i,j>3 \qquad \text{(A4b)}$$

Appendix B. Transformation Matrix

The transformation matrix T relates the local coordinate system of the inclusion $\left(x_{1'}, x_{2'}, x_{3'}\right)$ to the global coordinate system $\left(x_1, x_2, x_3\right)$ and is given by:[17]

$$T = \begin{bmatrix} T_{11} & T_{12} \\ T_{21} & T_{22} \end{bmatrix}$$

$$T_{11} = \begin{bmatrix} r_{11}^{\,2} & r_{12}^{\,2} & r_{13}^{\,2} \\ r_{21}^{\,2} & r_{22}^{\,2} & r_{23}^{\,2} \\ r_{31}^{\,2} & r_{32}^{\,2} & r_{33}^{\,2} \end{bmatrix}$$

$$T_{12} = 2\begin{bmatrix} r_{11}r_{12} & r_{11}r_{13} & r_{12}r_{13} \\ r_{21}r_{22} & r_{21}r_{23} & r_{22}r_{23} \\ r_{31}r_{32} & r_{31}r_{33} & r_{32}r_{33} \end{bmatrix}$$

$$T_{21} = \begin{bmatrix} r_{11}r_{21} & r_{12}r_{22} & r_{13}r_{23} \\ r_{11}r_{31} & r_{12}r_{32} & r_{13}r_{33} \\ r_{21}r_{31} & r_{22}r_{32} & r_{23}r_{33} \end{bmatrix}$$

$$T_{22} = \begin{bmatrix} r_{11}r_{22} + r_{12}r_{21} & r_{11}r_{23} + r_{13}r_{21} & r_{12}r_{23} + r_{13}r_{22} \\ r_{11}r_{32} + r_{12}r_{31} & r_{11}r_{33} + r_{13}r_{31} & r_{12}r_{33} + r_{13}r_{32} \\ r_{21}r_{32} + r_{31}r_{22} & r_{21}r_{33} + r_{23}r_{31} & r_{22}r_{33} + r_{23}r_{32} \end{bmatrix} \quad \text{(B1)}$$

where,

$$\begin{aligned} r_{11} &= \cos\alpha_1 \cos\alpha_3 - \sin\alpha_1 \cos\alpha_2 \sin\alpha_3 \\ r_{12} &= \sin\alpha_1 \cos\alpha_3 + \cos\alpha_1 \cos\alpha_2 \sin\alpha_3 \\ r_{13} &= \sin\alpha_2 \sin\alpha_3 \\ r_{21} &= -\cos\alpha_1 \sin\alpha_3 - \sin\alpha_1 \cos\alpha_2 \cos\alpha_3 \\ r_{21} &= -\sin\alpha_1 \sin\alpha_3 + \cos\alpha_1 \cos\alpha_2 \cos\alpha_3 \quad \text{(B2)} \\ r_{23} &= \sin\alpha_2 \cos\alpha_3 \\ r_{31} &= \sin\alpha_1 \sin\alpha_2 \\ r_{32} &= -\cos\alpha_1 \sin\alpha_2 \\ r_{33} &= \cos\alpha_2 \end{aligned}$$

Acknowledgments

The authors would like to thank Dr. Vernon Bechel of the Air Force Research Laboratory, Wright-Patterson for his technical guidance and support of the present work. This work is supported by the U. S. Air Force under Contract No. HQ0006-04-C-7070. Any opinions, findings and conclusions or recommendations expressed in this material are those of the author(s) and do not necessarily reflect the views of the U.S. Air Force.

References

1. Mallick, K. et al., "An Integrated Systematic Approach to Linerless Composite Tank Development," AIAA paper 2005-2089, 46th AIAA/ASME/ASCE/AHS/ASC Structures, Structural Dynamics & Materials Conference, Austin, Texas, 18 - 21 April 2005.
2. Mallick, K. et al., "Ultralight Linerless Composite Tanks for In-Space Applications," presented at the AIAA Space 2004 Conference, San Diego, Sept. 27-30, 2004.
3. Robinson, M. J., "Composite Cryogenic Tank Development", 35th AIAA Structures, Structural Dynamics, and Materials Conference and Adaptive Structures Forum, South Carolina, April 18-21,1994.
4. Adams, D. S., Bowles, D. E. and Herakovich, C. T. "Thermally Induced Transverse Cracking in Graphite-Epoxy Cross-Ply Laminates", Journal of Reinforced Plastics and Composites, Vol. 5, 1986, p 152.
5. Bechel. V., Through-Laminate Damage in Cryogenically Cycled Polymer Composites, AIAA-2004-1771 45th AIAA/ASME/ASCE/AHS/ASC Structures, Structural Dynamics and Materials Conference, Palm Springs, California, Apr. 19-22, 2004.
6. Bechel, V. T., "Permeability and Damage in Unloaded Cryogenically Cycled PMCs," AIAA paper 2005-20156, 46th AIAA/ASME/ASCE/AHS/ASC Structures, Structural Dynamics & Materials Conference, Austin, Texas, 18 - 21 April 2005.
7. Bechel, V. Negilski, M. and James, J., "Limiting the Permeability of Composites for Cryogenic Application", to be published in *Composites Science and Technology*, 2006.
8. Bechel V, Kim R. Y. , "Damage trends in cryogenically cycled carbon/ polymer composites", *Composites Science and Technology*, 2004, Vol. 64, pp.1773–84.
9. Gates, T. S., Grenoble R. W, Whitley K. S., "Permeability and life-time durability of polymer matrix composites for cryogenic fuel tanks", AIAA 2004-1859, 45th AIAA/ASME/ASCE/AHS/ASC SDM conference, Palm Spring, CA, 2004.
10. Yokozeki T, Aoki T, Ishikawa T., "Experimental cryogenic gas leakage through damaged composite laminates for propellant tank application", *Journal of Spacecraft Rockets,* 2005, Vol. 42(2), pp. 363–366.
11. Mallick, K., Tupper, M. L., Arritt, B. J. and Paul C., "Thermo-micromechanics of Microcracking in a Composite Cryogenic Pressure Vessel", 44th AIAA/ASME/ASCE/AHS/ASC Structures, Structural Dynamics & Materials Conference, 7-10 April 2003, Norfolk, Virginia.
12. Z. Hashin . "Analysis of Composite Materials - A Survey"; Journal of Applied Mechanics, 1983, Vol. 50, pp. 481-505.
13. S. Nemat-Nasser and M. Hori, "Elastic Solids with Microdefects" in Micromechanics and Inhomogeneity – The Toshio Mura Anniversary Volume, G. J. Weng et. Al., eds., 1990, Springer Verlag, New York, pp. 297-320.
14. D. Sumarac, D. Krajcinovic and K. Mallick, "Elastic Parameters of Brittle, Elastic Solids Containing Slits – Mean Field Theory", *International Journal of Damage Mechanics*, 1992, Vol. 1, pp. 320-346.
15. Takao, Y. and M. Taya, "Thermal Expansion Coefficients and Thermal Stresses in an Aligned Short Fiber Composite with Application to a Short Carbon Fiber/Aluminum", *Journal of Applied Mechanics*, 1985, Vol. 52, pp. 806-810.
16. Takao, Y. "Thermal Expansion Coefficients of Misoriented Short-Fiber Reinforced Composites", in "Recent Advances in Composites in the United States and Japan", J. R. Vinson, N. L. Taya (eds.), ASTM STP 864, 1985, pp. 685- 699.
17. G. M. Odegard and T. S. Gates, "Constitutive Modeling of Nanotube/Polymer Composites with Various Nanotube Orientations", 2002 SEM Annual Conference and Exposition on Experimental and Applied Mechanics, June 10-12, 2002, Milwaukee, WI.
18. D. Stauffer, "Introduction to Percolation Theory", 1985, Taylor & Francis, London.
19. I. Balberg, "Recent Developments in Continuum Percolation", *Philosophical Magazine B*, 1987, Vol. 56, No. 6, pp. 991-1003.
20. Clyne, T. W. and Withers, P. J., "An Introduction to Metal Matrix Composites", Cambridge University Press, 1993.
21. J. S. O. Evans, T. A. Mary, T. Vogt., M. A. Subramanian and A. W. Sleight, "Negative Thermal Expansion in ZrW_2O_8 and HfW_2O_8", *Chemical Materials*, 1996, Vol. 8, pp. 2809-2823.
22. D. K. Balch and D. C. Dunand, "Copper-Zirconium Tungstate Composites Exhibiting Low and Negative Thermal Expansion Influenced by Reinforcement Phase Transformations", *Metallurgical and Materials Transactions A*, 2004, Vol. 35A, pp. 1159.
23. Weyer, W. et al., "Achieving Dimensional Stability using Functional Fillers", AIAA paper 2005-2091, 46th AIAA/ASME/ASCE/AHS/ASC Structures, Structural Dynamics & Materials Conference, Austin, Texas, 18 - 21 April 2005.